Identifying drivers of streamflow extremes in West Africa to inform a nonstationary prediction model

Kwok Pan Chun, Bastien Dieppois, Qing He, Moussa Sidibe, Jonathan Eden, Jean-Emmanuel Paturel, Gil Mahé, Nathalie Rouché, Julian Klaus, and Declan Conway

Original citation & hyperlink:
Chun, K.P., Dieppois, B., He, Q., Sidibe, M., Eden, J., Paturel, J.E., Mahé, G., Rouché, N., Klaus, J. and Conway, D., 2021. Identifying drivers of streamflow extremes in West Africa to inform a nonstationary prediction model. *Weather and Climate Extremes*, *33*, 100346.
https://dx.doi.org/10.1016/j.wace.2021.100346

DOI 10.1016/j.wace.2021.100346
ISSN 2212-0947

Publisher: Elsevier

Weather and Climate Extremes 33 (2021) 100346

Contents lists available at ScienceDirect

Weather and Climate Extremes

journal homepage: www.elsevier.com/locate/wace

Identifying drivers of streamflow extremes in West Africa to inform a nonstationary prediction model

Kwok Pan Chun [a,*], Bastien Dieppois [b,c], Qing He [a], Moussa Sidibe [d], Jonathan Eden [b], Jean-Emmanuel Paturel [e], Gil Mahé [e], Nathalie Rouché [e], Julian Klaus [f], Declan Conway [g]

[a] Department of Geography, Hong Kong Baptist University, Hong Kong
[b] Centre for Agroecology, Water and Resilience (CAWR), Coventry University, UK
[c] Department of Oceanography, University of Cape Town, Cape Town, South Africa
[d] West African Science Service Centre on Climate Change and Adapted Land Use (WASCAL), Ouagadougou, Burkina Faso
[e] HydroSciences Montpellier (HSM), IRD, Montpellier, France
[f] Catchment and Eco-hydrology Research Group, Department of Environmental Research and Innovation, Luxembourg Institute of Science and Technology, Esch/Alzette, Luxembourg
[g] Grantham Research Institute on Climate Change and the Environment, London School of Economics (LSE), London, UK

ARTICLE INFO

Keywords:
Tropical indian ocean (TIO)
Eastern mediterranean (EMED)
Floods
Streamflow extremes
Nonstationary extreme model
West africa

ABSTRACT

West Africa exhibits decadal patterns in the behaviour of droughts and floods, creating challenges for effective water resources management. Proposed drivers of prolonged shifts in hydrological extremes include the impacts of land-cover change and climate variability in the region. However, while future land-degradation or land-use are highly unpredictable, recent studies suggest that prolonged periods of high-flows or increasing flood occurrences could be predicted by monitoring sea-surface temperature (SST) anomalies in the different ocean basins. In this study, we thus examine: i) what ocean basins would be the most suitable for future seamless flood-prediction systems; ii) how these ocean basins affect high-flow extremes (hereafter referred as extreme streamflow); and iii) how to integrate such nonstationary information in flood risk modelling. We first use relative importance analysis to identify the main SST drivers modulating hydrological conditions at both interannual and decadal timescales. At interannual timescales, Pacific Niño (ENSO), tropical Indian Ocean (TIO) and eastern Mediterranean (EMED) constitute the main climatic controls of extreme streamflow over West Africa, while the SST variability in the North and tropical Atlantic, as well as decadal variations of TIO and EMED are the main climatic controls at decadal timescales. Using regression analysis, we then suggest that these SST drivers impact hydrological extremes through shifts in the latitudinal location and the strength of the Intertropical Convergence Zone (ITCZ) and the Walker circulation, impacting the West African Monsoon, especially the zonal and meridional atmospheric water budget. Finally, a nonstationary extreme model, with climate information capturing regional circulation patterns, reveals that EMED SST is the best predictor for nonstationary streamflow extremes, particularly across the Sahel. Predictability skill is, however, much higher at the decadal timescale, and over the Senegal than the Niger catchment. This might be due to stronger impacts of land-use (-cover) and/or catchment properties (e.g. the Inner Delta) on the Niger River flow. Overall, a nonstationary framework for floods can also be applied to drought risk assessment, contributing to water regulation plans and hazard prevention, over West Africa and potentially other parts of the world.

1. Introduction

Droughts and floods are responsible for approximately 80% of fatalities, and around 70% of economic losses that are related to natural hazards in sub-Saharan Africa (Vicente-Serrano et al., 2012). West Africa has experienced persistent droughts since the end of the 1960s, with extreme droughts in 1972–1973 and 1983–1984 (Dai et al., 2004; Dezfuli and Nicholson, 2012). While the persistent droughts resulted in decreasing surface flows in some areas (Olivry, 2002; Descroix et al., 2013; Mahe et al., 2013), many catchments presented increased surface

* Corresponding author.
E-mail address: kpchun@hkbu.edu.hk (K.P. Chun).

https://doi.org/10.1016/j.wace.2021.100346
Received 12 June 2020; Received in revised form 24 June 2021; Accepted 29 June 2021
Available online 30 June 2021

flows in the Sahel (Séguis et al., 2002, 2011; Descroix et al., 2009; Mahé and Paturel, 2009). This phenomenon has been called the Sahelian Paradox, and is usually attributed to the combined influences of land use changes and climate variability, leading to vegetation degradation, changes in organic matter content in the soils and thus water-holding capacity (Séguis et al., 2004; Amogu et al., 2010; Gardelle et al., 2010).

Despite persistent widespread droughts, damaging floods have also occurred in the Sahelian region of West Africa, e.g. the 1996, 1998 and 2010, 2012 and 2013 floods in Niamey (Tarhule, 2005; Descroix et al., 2013; Sighomnou et al., 2013). This persistence in flood occurrence could be linked to the post-1990s prolonged increase in base flows in many regions of West Africa, especially in the central Sahel regions (Roudier et al., 2014; Sidibe et al., 2018). These recent changes in surface flow are consistent with a regional partial recovery in Sahel rainfall (Nicholson et al., 2000; Dai et al., 2004; Lebel and Ali, 2009; Masih et al., 2014), which has been associated with an increase in extreme rainfall (Taylor et al., 2017; Wilcox et al., 2018), increasing soil saturation and flood generation (Tramblay et al., 2014). Frequent flooding conditions have presented challenges for sustainable water management, ecosystem and human life for emerging West African countries (Nicholson, 2005; Gal et al., 2017). However, little has been done to understand the shifting patterns of extreme streamflow (i.e., high-flow or floods) over West Africa, as well as the underlying climate mechanisms.

Over West Africa, rainfall variability is driven by the West African Monsoon (WAM) system, which strongly depends on variations in global and regional sea-surface temperature (SST) and regional land-surface conditions at different timescales (e.g., Nicholson et al., 2000; Giannini et al., 2005; Lu and Delworth, 2005; Balas et al., 2007; Rodríguez-Fonseca et al., 2011; Dieppois et al., 2013; Dieppois et al., 2015a). At the interannual timescale, for instance, the WAM dynamic is mainly driven by the El Niño-Southern Oscillation (ENSO; e.g., Giannini et al., 2005; Rodríguez-Fonseca et al., 2015), the Atlantic Equatorial Mode (also referred to as Atlantic Nino; e.g., Losada et al., 2010; Rodríguez-Fonseca et al., 2011) and SST in the Mediterranean Sea (e.g., Rowell, 2003; Gaetani et al., 2010; Fontaine et al., 2011). At decadal timescales, West African rainfall variability is mainly driven by the Inter-decadal Pacific Oscillation (IPO) and/or the Pacific Decadal Oscillation (PDO), as well as the Atlantic Multi-decadal Oscillation (AMO) patterns (Biasutti et al., 2008; Mohino et al., 2011; Dieppois et al., 2013, 2015b). Persistent behaviour in rainfall across the Sahel has prompted research on development of multi-year rainfall forecasts (Sheen et al., 2017Sheen et al., 2017) and exploration of their application in various sectors (Ward and Conway, 2020Ward and Conway, 2020). In the region, streamflow variability is strongly linked to rainfall, and its associated teleconnections with SST modes (e.g., Mahé and Citeau, 1993), but with substantial modulations in terms of amplitude resulting from interactions with catchment properties (Sidibe et al., 2019Sidibe et al., 2019Sidibe et al., 2019). At some timescales (e.g. interannual and decadal) and for some regions, such as the Sahel at decadal timescales, streamflow variability, as well as the link to SST modes of variability, can, however, appear exacerbated compared to rainfall, suggesting increasing predictability skill (Sidibe et al., 2019). In addition, streamflow data integrates information about climate variability spatially, and are less sensitive to measurement errors than precipitation data, hence providing a greater signal-to-noise ratio (Chiew et al., 1998). Enhancing the prediction of decadal to multi-decadal fluctuations in streamflow is actually of crucial importance, as their magnitudes have been shown to be more important than the secular trends over the whole of West Africa (Sidibe et al., 2019). With the influence of the global and regional SST variabilities, patterns of extreme streamflow behaviour may exhibit further long-term memory in West Africa. However, despite early recommendations from regional authorities, e.g. AGRHYMET (Hamatan et al., 2004), the relative contributions and predictability skills of the different SST modes of variability to extreme streamflow (i.e. high-flow) conditions remain as yet unexplored over the region.

Modelling of streamflow extremes plays an essential role on the efficient design of water resources management (Schlef et al., 2018). Traditionally, studies of extreme conditions were conducted by stationary extreme models (e.g., Schlather, 2002; Ferro and Segers, 2003). However, stationary extreme models based on the assumption of the dynamics of invariant hydroclimate systems may no longer be valid in a changing climate. Therefore, multiple nonstationary extreme analysis approaches have been proposed for projecting hydrological extremes (e.g., Lima and Lall, 2010; Zhang et al., 2011; Cheng et al., 2014). This study uses nonstationary extreme analysis to account for potential changes in streamflow extremes over West Africa from one decade to another, and therefore provide more robust estimates of prolonged or multi-year high-flow (flood) conditions than stationary extreme modelling approaches. Apart from providing a more realistic estimate of extreme streamflow, this study also aims to identify the underlying climate mechanisms by exploring the nonstationary relationships between interannual and decadal SST variability and hydrological extreme distributions.

This involves examining the contributions (relative importance) of the different ocean basins to extreme streamflow variability at both interannual and decadal timescales; their larger-scale mechanisms are also investigated, in order to identify physically relevant information for nonstationary extreme modelling approaches, for estimating flood risks. The paper is structured as follows. In Section 2, we introduce the study region and data. In Section 3, the methodology, including relative importance analysis and extreme analysis, is presented. In Section 4.1, the most important SST indices contributing to extreme streamflow variability over West Africa, and the nonstationary extreme analysis driven by SST indices, are investigated. In Section 4.2, we assess the physical meaning of the statistical links between SST variability and high-flow extremes, by examining the effects of the most relevant SST indices on the atmospheric water budget, as well as their interdependencies between the SST variabilities of different oceans. In Section 4.3, we assess the performance of the nonstationary extreme models for extreme streamflow. In Section 5, the implications of our results and possible future applications of our approach for the predictability of streamflow extremes are summarized.

2. Study region and data

2.1. Study basins and streamflow data

The extreme analysis is based on in-situ streamflow observations of two major basins in West Africa: the Niger River basin (NRB) and Senegal River basin (SRB; Fig. 1). The NRB and SRB, located in Sudano-Guinean and Sahelian regions, are the first and second largest river basins in West Africa, with a drainage area of 2,170,500 km^2 and 300,000 km^2, respectively (Wilcox et al., 2018). Both basins are transboundary, supporting the irrigation and domestic water demands of large populations (Oyerinde et al., 2015; Wilcox et al., 2018). Daily streamflow data are collected from the SIEREM ("Système d'Informations Environnementales sur les Ressources en Eaux et leur Modélisation") database (Boyer et al., 2006). Only time series from stream gauges that are not affected by any upstream dams or reservoirs are selected from the GRanD database (Lehner et al., 2011). In addition, to ensure the robustness of our results, only the longest time series of stream gauge records presenting less than 30% of missing values over the 20th century and recent decades are investigated. However, it should be noted that missing data are most before 1950. For more detail, the list of stations, their geographic coordinates and record periods of the stations are given in Table 1.

2.2. Sea-surface temperature data

We use a global monthly gridded dataset, the Extended Reconstructed SST version 5 (ERSST.v5; Huang et al., 2017), which is derived

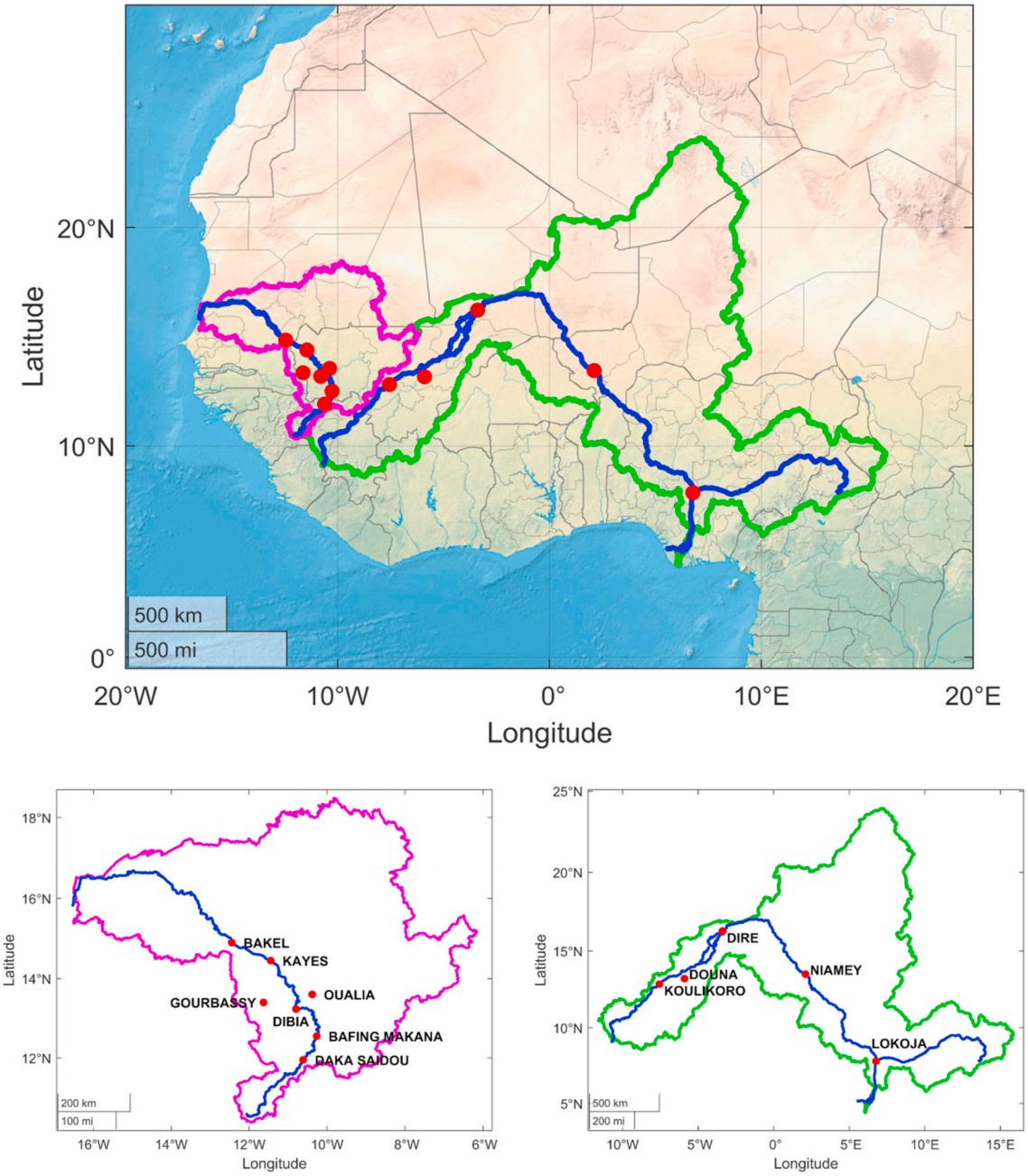

Fig. 1. Locations of 12 streamflow stations in the NRB (green boundary) and SRB (magenta boundary). The red dots represent the streamflow stations, and the blue lines are the main river channels.

Table 1
List of stations, station locations, missing data percentage, start and end time.

Basin (Tributary)	station	start	end	missing data (%)	latitude	longitude
Niger	Dire	January 01, 01/01/1924	May 23, 23/05/2017	1.88	16.27595	−3.395
Niger (Bani)	Douna	May 01, 01/05/1922	May 23, 23/05/2017	19.39	13.21385	−5.90311
Niger	Koulikoro	January 01, 01/01/1907	August 20, 20/08/2019	0.34	12.85727	−7.55811
Niger	Lokoja	October 01, 01/10/1914	October 30, 30/10/1960	1.65	7.8	6.7667
Niger	Niamey	January 01, 01/01/1929	May 23, 23/05/2017	9.95	13.5016	2.105
Senegal	Bafing Makana	June 15, 15/06/1903	October 29, 29/10/2006	6.67	12.55	−10.2667
Senegal	Bakel	January 05, 05/01/1904	February 28, 28/02/2005	22.45	14.9	−12.45
Senegal	Daka Saidou	June 14, 14/06/1903	October 29, 29/10/2006	0.73	11.95	−10.6167
Senegal	Dibia	June 16, 16/06/1903	January 30, 30/01/1995	0.00	13.2333	−10.8
Senegal (Faleme)	Gourbassy	June 17, 17/06/1903	March 28, 28/03/2005	0.00	13.4	−11.6333
Senegal	Kayes	July 01, 01/07/1903	February 28, 28/02/2005	28.52	14.45	−11.45
Senegal (Bakoye)	Oualia	June 15, 15/06/1903	February 28, 28/02/2005	8.85	13.6	−10.3833

from the International Comprehensive Ocean–Atmosphere Dataset (ICOADS) Release 3.0, to infer SST variability in the different ocean basins. This dataset spans from January 1854 to the present at a $2^\circ \times 2^\circ$ grid resolution, and has improved SST spatial and temporal variability through new reconstruction methods, especially related to the use of Empirical Orthogonal Teleconnections (Huang et al., 2017). More importantly, unlike other SST datasets, ERSST. v5 is not affected by cold SST biases resulting from satellite data assimilation at the end of the 20th century, which can sometimes induce a modest decrease in the global warming trend and problematic negative decadal signals (Reynolds et al., 2002).

Table 2 lists ten SST indices representative of the ocean regions linked to Sahel rainfall and streamflow variability at interannual and decadal timescales (Fontaine et al., 2011; Rodríguez-Fonseca et al., 2011, 2015; Dieppois et al., 2015a; Sidibe et al., 2019). The SST indices are calculated using Empirical Orthogonal Functions (EOFs) from the regions where different modes of SST variability could interact. SST anomalies (SSTa), weighted by the square root of cosine of latitudes and averaged over the corresponding regions, are calculated by suppressing the monthly cycle and detrending the data. In addition, a quasi-global SST (GT) index is also defined as an oceanic proxy of the global SST evolution (Trenberth and Shea, 2006), and is calculated as follows:

$$GT(t) = \frac{\sum_{i=1}^{n} SSTa_i^{'}(t) \times \sqrt{\cos(\theta)}}{n} \quad (1)$$

where n is the number of grid points considered, and θ is the latitude. To optimise the representation of regional mode of SST variability, the GT influence is removed from each SST indices by subtracting linear regressions. This operation can be summarizsed as:

$$SSTa(\theta, \varphi, t) = SSTa^{'}(\theta, \varphi, t) - GT(t) \quad (2)$$

where φ is the longitude. $SSTa^{'}$ represent the original SST anomalies, and $SSTa$ are SST anomalies with GT influence removed. As recommended in Trenberth and Shea (2006), such a procedure is a more appropriate method for adjusting contemporary climate change effects from SSTa than simply removing a linear temporal trend over the reference period.

In addition, as the drivers of the WAM dynamic are known to vary according to the timescale, all SST indices are decomposed into two different timescales: interannual (2–8 years) and decadal (>10 years). To account for changes in the contributions of interannual and decadal variability throughout the year, the time series are decomposed monthly using fast Fourier transform (FFT) band-pass filtering, which can be considered a digital filter in frequency domain, before being aggregated annually. The time series are detrended prior to the FFT filtering using a locally weighted linear regression; a nonzero mean and the trend term may otherwise affect the results (Wu et al., 2007).

Table 2
Detailed information for ten SST indices.

Region	SST index	Description	References
Global	GT	Weighted global SSTa (-70-70°N)	Trenberth and Shea (2006)
Atlantic	AtlNiño	1st principal component (PC) of tropical Atlantic SSTa (-70-20°E, -30-30°N)	Chiang and Vimont (2004)
	AMM	2nd PC of tropical Atlantic SSTa (-70-20°E, -30-30°N)	Chiang and Vimont (2004)
	AMO	Average SSTa for the North Atlantic (-80-0°E, 0–60°N)	Enfield et al. (2001); Trenberth and Shea (2006)
Mediterranean Sea	EMED	Average SSTa for the East Mediterranean (15–36°E, 32–44°N)	Fontaine et al. (2011)
	WMED	Average SSTa for the West Mediterranean (-6-15°E, 32–44°N)	Fontaine et al. (2011)
Pacific	ENSOpc	1st PC of equatorial Pacific SSTa (110°E– 95°W, -30-30°N)	Saji et al. (2006); Cai et al. (2009); Weller and Cai (2013)
	IPOpc	1st PC of Pacific SSTa (100°E– 70°W, -50-50°N)	Folland et al. (1999); Power et al. (1999)
	PDOpc	1st EOF of North Pacific SSTa (100°E– 100°W, 20–65°N)	Mantua et al. (1997)
Indian	TIO	Average SSTa for the Tropical Indian Ocean (35–90°E, -24-24°N)	Fontaine et al. (2011)

2.3. Atmospheric data

We use the Twentieth Century Reanalysis version 3 (20 C RCR.v3; Compo et al., 2011; Slivinski et al., 2019) to examine regional to global atmospheric anomalies impacting the atmospheric water budget over the region. The 20 C RCR.v3 is an 80-member ensemble global reanalysis (from 1806 to 2015) dataset at a $1^\circ \times 1^\circ$ grid resolution. This reanalysis product only assimilates surface pressure observations with monthly SST and sea-ice distributions as boundary conditions. This modelling and data assimilation strategy is constant over the entire period, and allows for spectral decomposition in the analyses of atmospheric circulation across different timescales, with a reduced sensitivity to artificial shifts induced by assimilation of new datasets – as is the case for the NCEP/NCAR-1 reanalysis as shown in Poccard et al. (2000). The density of the observational network required for assimilation, as well as the quality of the SST field used as boundary conditions, remain nevertheless difficult issues, especially for the 19th century and the 1st-half of the 20th century (Pohl et al., 2018). Compared to 20CRv2c, where these issues lead to different shortcomings in global sea-level pressure, precipitation and winds, 20CRv3 uses new adaptive data assimilation methods, a new higher-resolution forecast model that specifies dry air mass and assimilates a larger set of pressure observations to optimally reduce those shortcomings (Slivinski et al., 2019). However, it is noted that our results could be slightly different if the analysis was based on another century-long reanalysis, such as ERA-20C (Poli et al., 2016) and CERA-20C (Laloyaux et al., 2018), which are based on similar assimilation data but different atmospheric models (Wohland et al., 2019). Nevertheless, according to Berntell et al. (2018), 20CRv2 is better representing decadal rainfall variability in the Sahel, as compared to ERA-20C and CERA-20C, in which decadal signals are significantly negatively correlated to the observation. In addition, this study can be compared to other studies based on 20CRv3 to analyse the atmospheric dynamic associated with interannual to decadal variability in Sahel rainfall (Fontaine et al., 2011; Dieppois et al., 2013) and streamflow (Sidibe et al., 2019).

In this study, at interannual and decadal timescales, we use integrated moisture flux (Vq) and convergence at two different levels to account for vertical wind shear over the region: lower-troposphere (i.e. 1000-800 h PahPa: monsoon layer) and mid-troposphere (i.e. 800-500 h PahPa: African Easterly Jet [AEJ] layer). This gives a synthetic representation of horizontal water movements within West African monsoon circulation, as these two levels represent ~97% of moisture content of the total atmospheric column (i.e. from 1 000 to 1 h PahPa) over the region (not shown). In addition, to estimate the vertical water movements, we examine outgoing longwave radiation (OLR) at the nominal top of the atmosphere. In the tropics, OLR anomalies can be used as a proxy for deep-convection processes: negative (positive) OLR anomalies are associated with enhanced (suppressed) deep-convection.

3. Methodology

3.1. Relative importance analysis

To identify which SST indices are the most important contributors to

streamflow extremes over the two main river basins of West Africa, relative importance analysis is applied. Relative importance analysis consists of decomposing the coefficient of determination (R^2) and quantifying the contribution of each regressor to the total R^2 in a linear regression model. For relative importance application in streamflow analysis, various methods have been proposed. Using the Lindeman, Merenda and Gold (LMG) approach (Lindeman et al., 1980), Tyralis et al. (2019) explained the shape parameter of the Generalised Extreme Value (GEV) distribution of streamflow extremes in a static context. Here, we use one of the most popular relative importance methods, the proportional marginal variance decomposition (PMVD; Feldman, 2005) which is similar to the LMG methods, but the PMVD weights depend on the order of variable inclusion in the correlation decomposition algorithm. The PMVD is based on sequential R^2, but eliminates the dependence of each regressor's contribution on orderings by averaging all marginal contributions (Grömping, 2007). The marginal contribution (M_i) of a regressor (X_i) is defined as:

$$M_i = R^2(X_i|S) = R^2(\{X_i\} \cup S) - R^2(S) \tag{3}$$

where S represents the set of regressors entered into the model. However, the marginal contribution of a regressor is influenced by its order in the model. The order of $X_1, \cdots, X_P$ into the model can be denoted as $r = (r_1, \cdots, r_P)$, and then the set of regressors entered into the model before X_i according to the order r is denoted as S_i^r. The marginal contribution (M_i) of a regressor (X_i) in the order r can be expressed as:

$$M_i = seqR^2\left(X_i|S_i^r\right) = R^2\left(\{X_i\} \cup S_i^r\right) - R^2\left(S_i^r\right) \tag{4}$$

Then the PMVD can be written as:

$$PMVD(X_i) = \frac{1}{p!} \sum_{rpermutation} w(r) seqR^2\left(X_i|S_i^r\right) \tag{5}$$

where $seqR^2(X_i|S_i^r)$ indicates sequential marginal contribution of the regressor (X_i) in the order r and $w(r)$ indicates the data-dependent PMVD weights in the permutation r. The weights are derived based on a set of axioms. For a proper exclusion, we set a regressor with an actual zero coefficient to have a zero share of the R^2. For this study, this procedure is applied at both interannual and decadal timescales using the most relevant indices at those timescales (cf. Rodríguez-Fonseca et al., 2011; Rodríguez-Fonseca et al., 2015).

3.2. Regression analysis

To understand further the physical meaning of the link between SST indices and streamflow extremes at interannual and decadal scales, the SST indices have been linearly regressed on larger-scale climate data between 1901 and 2015. We first examine the global SST patterns associated with each SST index to assess interdependency across SST indices. Then, we examine the low-to mid-tropospheric moisture fluxes, as well as the OLR anomalies, related to those global SST patterns to determine the horizontal and vertical fluxes of water over the region, and their association with global circulation.

To provide a quantitative evaluation of regression results, statistical significance is estimated using two tests: i) a local random-phase test accounting for serial correlations (Ebisuzaki, 1997); ii) a global or field significance test, based on the false discovery rate (FDR), accounting for spatial auto-correlation and the problem of multiplicity (Wilks, 2006, 2016). For each pair of time series to be regressed (a and b), 10,000 random time series having the same power spectrum as the original one, but random phases, are regressed. The significance is then estimated as follows: if fewer than $\alpha \times 100\%$ of the regressions (r_{ab}) from the random-phase series have a magnitude greater than the critical value r_{crit}, the null hypothesis is rejected at the α significance level whenever $|r_{ab}| > r_{crit}$. The resulting p-values (p) are then adjusted using the global FDR test at $p = 0.05$ to control the expected proportion of locally significant tests that are actually true, and not occurring by chance. Hence, field significance is determined if at least one local null hypotheses is rejected according to this criterion at the level $\alpha_{global} = 0.05$ (Wilks, 2006, 2016). We reject a local test if p_{local} is no greater than:

$$P_{FDR} = \max_{j=1\to k} \left\{ p_{local}(j) : p_{local}(j) \leq \alpha_{global} \left(\frac{j}{k}\right) \right\} \tag{6}$$

where p_{local} (j) denotes the jth smallest (out of k) local p values.

3.3. Extreme analysis

For the estimation and extrapolation of future extreme streamflow over the two basins, the extreme analysis is applied to daily streamflow measurements. Three points are the most important for extreme analysis, including the selection of probability distributions, stationarity assumptions and distribution estimation methods (Pisarenko and Rodkin, 2010). The GEV distribution has been demonstrated to be very suitable for environmental extreme analysis, since it contains the family of extreme distributions (e.g., Rust et al., 2009; Maraun et al., 2010; Tošić et al., 2017), and is used here. However, before applying the GEV distribution, a block maxima approach, with a length equal to a year, is used to obtain the extreme values; annual consideration should be sufficient for our more than 70-year long time series (Kotz and Nadarajah, 2000; Katz et al., 2002; Hawkes et al., 2008). Considering a sequence of daily streamflow observations $X_t (t = 1, 2, \ldots, N)$ from the whole period, the block maxima can be written as:

$$B_n = max\{X_1, X_2, \ldots, X_N\} \tag{7}$$

For increasing block length $(N \to \infty)$, the distribution of block maxima B_n converges to a non-degenerate probability distribution functions (PDF), which is the GEV distribution. It is of the form:

$$GEV(z; \mu, \sigma, \varepsilon) = \exp\left(- \left[1 + \varepsilon\left(\frac{z-\mu}{\sigma}\right)\right]_+^{-\frac{1}{\varepsilon}} \right) \tag{8}$$

where the operation of $a_+ = max(0, a)$, μ is the location parameter, σ is the scale parameter and ε is the shape parameter. When the shape parameter ε is zero, the GEV distribution becomes the Gumbel distribution. Equation (8) describes the stationary extreme model, which is still used for comparison with the nonstationary GEV. The nonstationary GEV at time t is, as:

$$GEV(x(t); \mu(t), \sigma(t), \varepsilon(t)) = \exp\left(- \left[1 + \varepsilon(t)\left(\frac{x(t)-\mu(t)}{\sigma(t)}\right)\right]_+^{-\frac{1}{\varepsilon(t)}} \right) \tag{9}$$

where the non-negative operation of $a_+ = max(0, a)$. $\mu(t)$, $\sigma(t)$ and $\varepsilon(t)$ are the time varying location, scale and shape parameters, respectively. To show the nonstationarity of hydrological conditions in a changing climate, previous studies have suggested linking the distribution parameters and hydroclimate variability, such as precipitation (Šraj et al., 2016), monsoon activity (Delgado et al., 2014), atmosphere circulation patterns (Wilby and Quinn, 2013) and SST oscillations (Zhang et al., 2010; Lü et al., 2018). In this study, nine SST indices at interannual and decadal timescales are taken as covariates for the location and scale parameters; the shape parameter is not covariate-dependent and remains stationary.

For the parameter estimation, calibration and validation, the L-moment (Hosking, 1990) and maximum likelihood (Coles, 2001) are common choices. The L-moment is suitable for short time series (Delicado and Goria, 2008), while maximum likelihood performs well for large-sample parameter estimation (Martins and Stedinger, 2000). Given that the period of analysis is around 70 years, the maximum likelihood is chosen. There is no analytical solution for the nonstationary maximum likelihood estimates; and the Newton-Raphson method is

used to get unbiased maximum likelihood estimates. Also, the nonstationary parameter standard errors and their confidence intervals are estimated from the observed information matrices based on approximate normality of the maximum likelihood estimation.

The significance of the estimated GEV parameters has then been assessed using the Leave-X-out cross-validation (LXOCV) approach, which consists of validation sets which X observations are not from training sets (Celisse, 2014). To select the appropriate length of data (i.e., total length of data minus *X*) for parameter estimation, 1 000 simulations of different lengths (20, 30, 40, 50, 60 and 70) are tested. When the data length is longer than 60 years, the estimated parameters are significant (Figure A1). However, where our record is shorter than 60 years, it is more likely to obtain nonsignificant results (Figure A1). In this study, there are around 70 years of data, thus, to obtain significantly stable parameters, the *p* value has to be at most around 40. Different combinations for parameter nonstationarity with the nine SST indices are considered (e.g., location parameter μ is changing with EMED: $\mu(EMED)$). The performance for extreme model predictions of different combinations is then assessed based on the root mean squared error skill score (SS_{RMSE}) (Jolliffe and Stephenson, 2012). The SS_{RMSE} is used to measure the closeness of the model and observations over a long time period (Tao et al., 2014), and it can be written as:

$$SS_{RMSE} = \left(1 - \frac{RMSE_{non}}{RMSE_{sta}}\right) \times 100\% \quad (10)$$

where $RMSE_{non}$ ($RMSE_{sta}$) is the root mean squared error of observation compared to the nonstationary (stationary) modelled results. Note that here the stationary model is used as the reference prediction. A higher SS_{RMSE} value indicates that a nonstationary model is more skilful for prediction. The negative SS_{RMSE} value shows cases where a nonstationary model has less prediction skill than its referenced model (i.e., stationary model).

4. Results and discussion

4.1. Relative importance of SST indices to extreme streamflow variability

Fig. 2 displays the most important contributors to streamflow extremes, at both interannual and decadal timescales, over the two main river basins of West Africa. At the interannual timescale, the predictability skill varies greatly, especially over the NRB, where it fluctuates from 6.7% at Douna on the Bani (Niger tributaries) to 39.5% at Koulikoro upstream of the inner Niger Delta (Fig. 2a). Except for Oulia on the Bakoye (Senegal tributaries), predictability skills remain moderately good, ranging from 18.4% to 25.8%, over the SRB (Fig. 2a). Both the Atlantic and Pacific ENSO variability, *i.e.* AtlNiño and ENSOpc indices, are the main contributors to interannual variability of extreme streamflow (up to 10 and 12% of contributing variance, respectively; Fig. 2b). Interestingly the relative contribution of Atlantic and Pacific ENSO differs regionally: AtlNiño contributions are stronger over most of the SRB, while ENSOpc contributions are greater over the Sahelian part, downstream of the inner Niger Delta (Fig. 2b). This is consistent with previous studies on Sahel rainfall, identifying the tropical Pacific and Atlantic Oceans as the leading drivers of interannual variability (Losada et al., 2010; Rodríguez-Fonseca et al., 2011). However, here, the Atlantic Meridional Mode (AMM) shows very little contribution to interannual variability in extreme streamflow (up to 2% only; Fig. 2b). According to previous studies on Sahel rainfall (Rowell, 2003; Fontaine

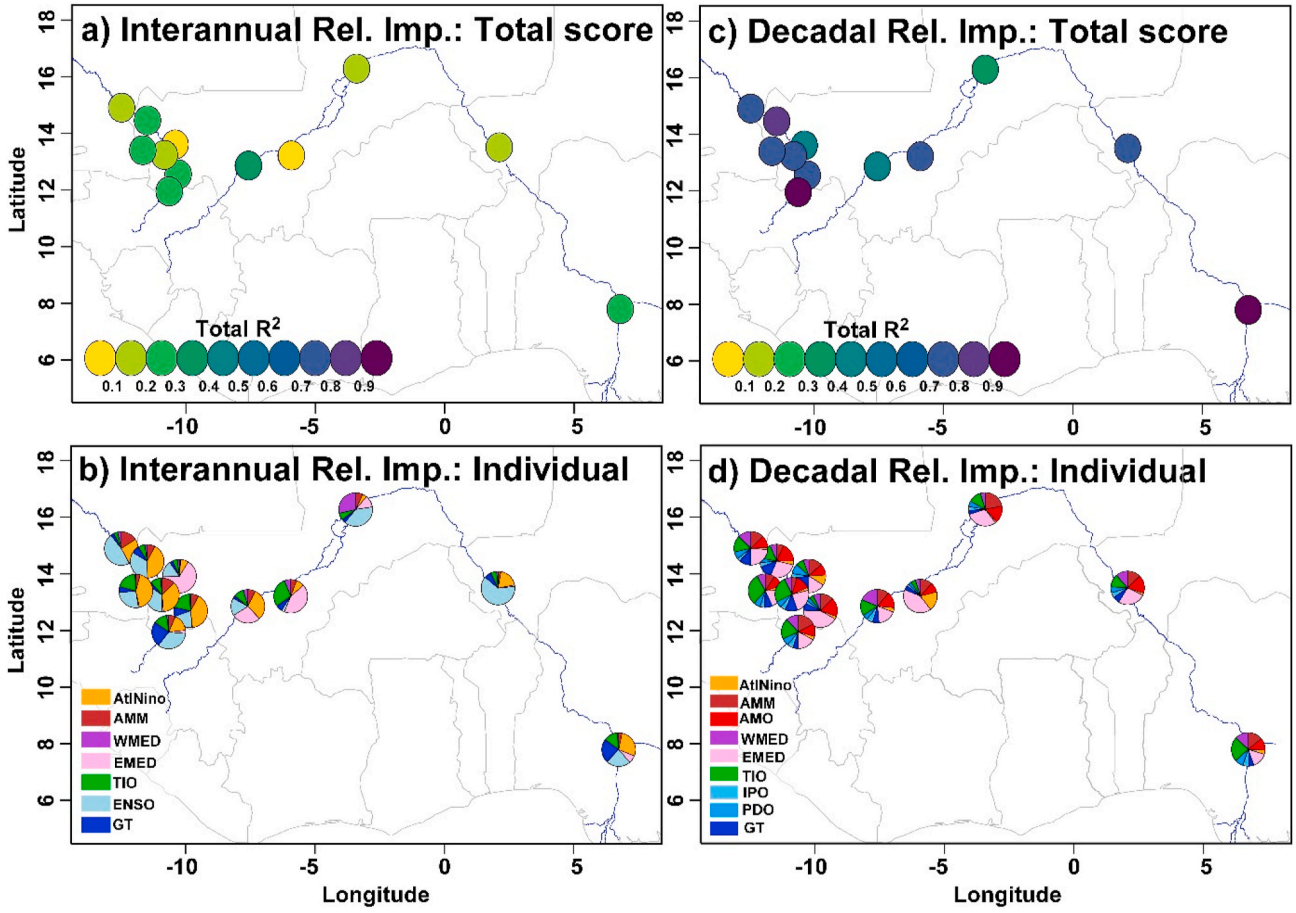

Fig. 2. The total coefficient of determination R^2 and relative importance of SST indices to extreme streamflow variability at interannual (a–b) and decadal scales (c–d). Colours in the pie charts refer to the total R^2 values and each SST indices' (regressor) contributions in a/c and b/d.

et al., 2010; Gaetani et al., 2010), eastern Mediterranean SSTa also contribute to interannual variability in streamflow extremes, especially for the upstream of the inner Niger Delta in Koulikoro, where it contributes up to 11% of extreme streamflow variance (Fig. 2b). Similarly, the Indian Ocean SSTa (TIO) shows moderate contributions to interannual extreme streamflow variability, especially over the western Sahel (up to 8% of contributing variance; Fig. 2b). This is consistent with Bader and Latif (2011), which demonstrated that the Indian Ocean SSTs were the main forcing for the drought over the west Sahel in 1983. However, as stated in Rodríguez-Fonseca et al. (2015), the interannual relationship between the Indian Ocean and Sahel rainfall has been infrequently studied, despite their crucial importance on the teleconnection with the Mediterranean (Fontaine et al., 2011) and Pacific Oceans (Rowell, 2001).

At the decadal timescale, predictability skills are much greater than at the interannual timescale, and vary from 45.2% to 91.5% (Fig. 2c). Such discrepancies in predictability skill are, however, consistent with findings from Sidibe et al. (2019), indicating that streamflow variability over the SRB and NRB is primarily dominated by decadal variability, expressing between 40 and 60% of the total annual streamflow variance. Mediterranean SSTa, in particular the eastern regions (EMED), substantially contribute to extreme streamflow variability in both watersheds (20–40% of contributing variance; Fig. 2d). Interestingly, the contributions of Mediterranean SSTa to decadal variability in extreme streamflow always exceed the contribution of the AMO, IPO and PDO, which were described as the primary driver of decadal rainfall variability over the Sahel (Mohino et al., 2011; Rodríguez-Fonseca et al., 2011, 2015). This, however, is consistent with sensitivity experiments in climate models, highlighting that either the North and the tropical Atlantic basins cannot solely control the overall precipitation structure at this timescale, and that SST forcing from the Mediterranean basin is required (Mohino et al., 2011). Here, the AMO, as well as the tropical Atlantic SST modes of variability (*i.e.* AtlNiño and AMM), show a moderate contribution to extreme streamflow variability at all stations (from 5 to 15% of contributing variance; Fig. 2d). The contributions of the Pacific Ocean to decadal variability in extreme streamflow, however, remain minor at all stations (Fig. 2d). Yet, this is also consistent with the sensitivity experiments by Mohino et al. (2011), which show that the relationship between the IPO and decadal rainfall anomalies over the Sahel is not solely driven by the Pacific, but by the entire tropical patterns, especially over the Indian Ocean. Thus, SSTa in the tropical Indian Ocean (TIO) show a larger contribution to decadal variability in extreme streamflow than the IPO and PDO, especially over the western Sahel where the contribution reaches 25% (Fig. 2d).

In summary, while predictability skills are low to moderately high at the interannual timescale, much greater skill is found at the decadal timescale, suggesting there is potential for seamless predictions of prolonged droughts and high-flow conditions over the region. Predictability skill, however, varies greatly at the regional scale, highlighting potential alterations of climate signals by catchment properties, as discussed in Sidibe et al. (2019), and other factors. Overall, the results are more consistent over the SRB than over the NRB. This might be due to the differences of catchment size and their bioclimatology. The NRB covers more diverse bio-climatic zones and is more heterogeneous than the SRB. Regarding the climate drivers, SSTa in the Pacific and tropical Atlantic Oceans primarily drive interannual variability in extreme streamflow, while decadal variability appears primarily driven by the Mediterranean Sea, the Atlantic Ocean (North and tropical) and the Indian Ocean.

4.2. Further understanding climate processes driving hydrological extremes

In this section, the most relevant SST indices contributing to interannual and decadal variability in hydrological extremes are selected to further analyse the physical meaning of statistical links identified in Section 4.1.

4.2.1. Interannual timescales

Based on the relative importance analysis, ENSO, AtlNiño, TIO and EMED are identified as the most relevant SST indices contributing to streamflow extreme variability at the interannual timescale (cf. Fig. 2b). Those SST indices have been regressed on global SSTa to check for interdependencies between ocean basins, tropical OLR anomalies and low- to mid-tropospheric moisture fluxes to examine vertical and horizontal water movements.

El Niño is significantly linked to positive OLR anomalies over West Africa, suggesting that suppressed deep-convection is embedded in the field of larger-scale OLR anomalies over the Pacific and Indian Oceans describing zonal shifts in the Walker circulation (Fig. 3a). In the lower troposphere (or Monsoon layer: 1 000-800 hPa), El Niño also relates to easterly and southerly moisture fluxes between the West African continent and the South Atlantic (Fig. 3a). In the mid-troposphere (or AEJ) layer: 750-500 hPa), El Niño is connected to easterly fluxes between the Equator and 10°N (Fig. 3a). The anomalies in horizontal moisture fluxes describe a weakening of the Monsoon fluxes and an enhancement of the AEJ activity, both driven by increasing moisture divergence (Fig. 3a). El Niño thus leads to a decrease in water supply from the equatorial Atlantic and an increase in continental moisture export to the Atlantic, both promoting drought conditions. Very similar climate anomalies are found with the TIO, which does not appear strictly independent to ENSO, but shows much stronger deep-convection anomalies and impacts over the western Sahel and southeast West Africa (Fig. 3c), consistent with the relative importance analysis (Fig. 2b).

The impact of Atlantic Niño is, however, restricted to the Gulf of Guinea coastal regions (GG: 4° to 10°N), where deep-convection is strongly promoted (Fig. 3b). In the lower troposphere, this enhanced deep-convection is linked to major anomalous southerly moisture fluxes between 10°N and the Equator, as well as anomalous northerly fluxes over the South Atlantic (Fig. 3b), which together describe a southward shift of the Intertropical Convergence Zone (ITCZ) and the WAM. In addition, we note a decrease of the AEJ activity in the mid-troposphere (Fig. 3b). Thus, at the interannual timescale, while the Pacific and Indian Oceans both modulate the strength of the WAM through zonal changes in vertical motion, increasing or decreasing moisture divergence, the Atlantic Ocean plays an important role in the meridional circulation, regulating the latitudinal location and strength of the ITCZ and the WAM.

Eastern Mediterranean SSTa, which are associated with a significant wave-like SST pattern over the North Atlantic, appear to play a role in the latitudinal location and strength of the ITCZ at the interannual timescale. Warmer eastern Mediterranean SSTa are significantly linked to enhanced deep-convection over the eastern Sahel, in response to increasing convergence between southwesterly moisture fluxes from the equatorial Atlantic, and northeasterly moisture fluxes from the eastern Mediterranean in the lower troposphere (Fig. 3d). Such lower tropospheric circulation anomalies act as a strengthening and a northward shift of the ITCZ and the WAM. In addition, mid-tropospheric anomalies reveal significant easterly moisture fluxes over eastern Africa (Fig. 3d), which contribute to reduced AEJ activity in exporting continental moisture toward the Atlantic over all the eastern regions.

4.2.2. Decadal timescales

At the decadal timescale, the AMO, AMM, TIO and EMED are identified as the most relevant SST indices contributing to the variability of extreme streamflow (cf. Fig. 2d). Fig. 4 shows how those SST indices are related to the regional and large-scale climate anomalies linked with atmospheric water budgets.

Decadal warming of the North Atlantic, describing positive phases of the AMO, does not show a significant link to deep-convection processes over the Sahel, using both local and global significance testing (Fig. 4a). The AMO, however, appears significantly linked to southwesterly

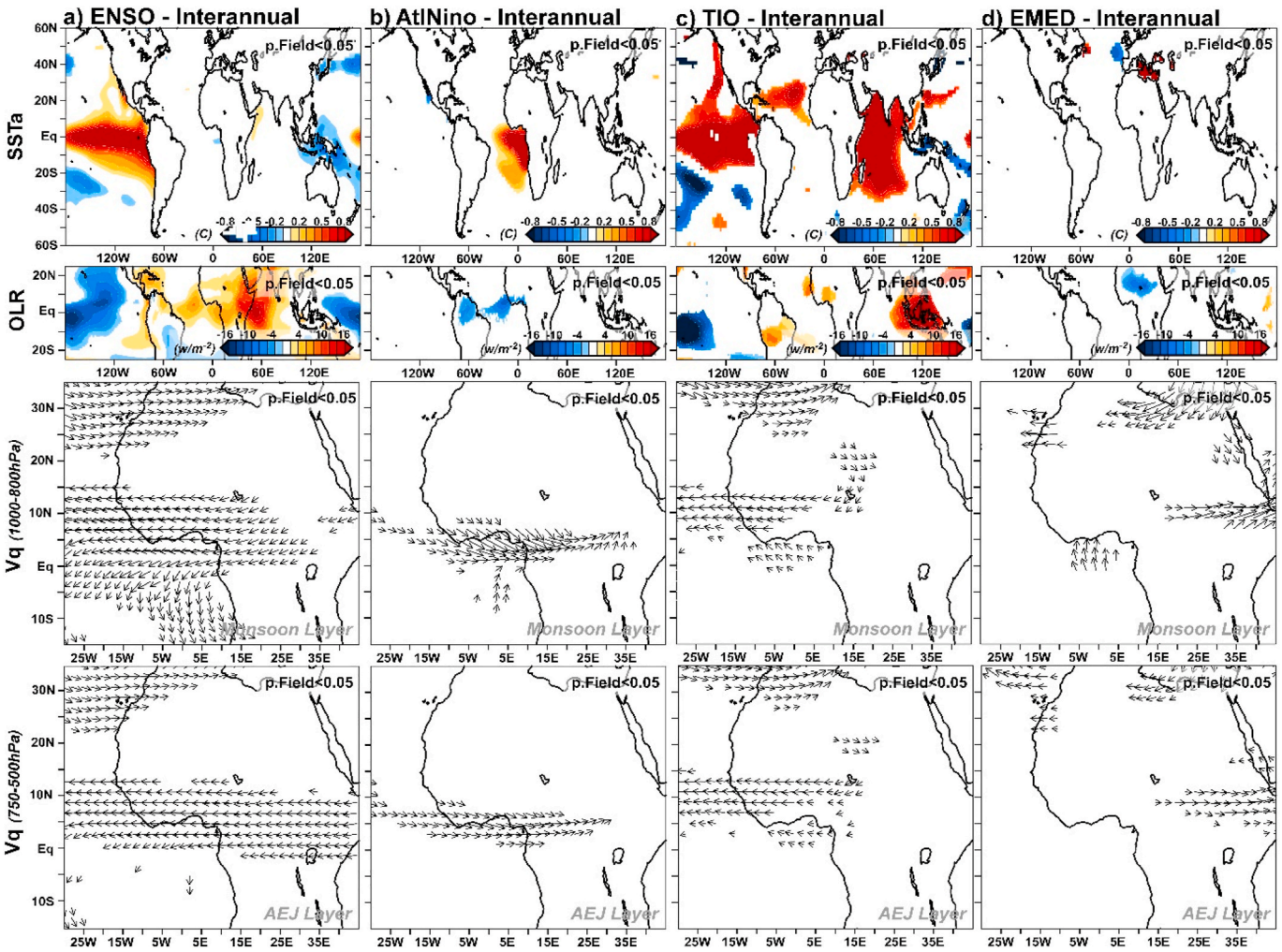

Fig. 3. Linear regressions between most relevant SST indices (a–d: ENSO, AtlNiño, TIO, EMED) and large-to regional-scale climate anomalies affecting the WAM variability at the interannual timescale (2–8 years; top to bottom: global SST, OLR, low- and mid-tropospheric moisture anomalies). Statistical significance is estimated using a local random-phase test accounting for serial correlations (Ebisuzaki, 1997), as well as a global FDR significance test (Wilks, 2006, 2016). Only significant regressions at $p \leq 0.05$ are shown.

moisture fluxes around 20°N (Fig. 4a), which could contribute to the enhanced convergence over the region. The AMM promotes deep-convection processes over the Sahel, and it shows much stronger links to the WAM (Fig. 4b). In addition, we note a weakening of moisture fluxes over the Azores High region (Fig. 4b), which has been shown to be linked to the Pacific SST variability (Gouirand et al., 2007), and a strengthened WAM (Grist and Nicholson, 2001, Fig. 4b). However, other studies also suggest that such a strengthened WAM could solely be linked to a warmer tropical North Atlantic and/or a colder Equatorial Atlantic (Losada et al., 2010; Rodríguez-Fonseca et al., 2011).

As at the interannual timescale, decadal variability in the TIO index is also strongly linked to Pacific SSTa, as well the Tropical North Atlantic (Fig. 4c), which is itself strongly related to variability in Pacific SSTa (García-Serrano et al., 2017). However, most atmospheric anomalies associated with decadal TIO variability are found to be not significant at $p \leq 0.05$ (up to $p \leq 0.2$) using both local and global significance testing (Fig. 4c). Therefore, the effects of TIO are not distinguishable from random noise, and this suggests that the strong relationship between TIO and extreme streamflow variability is not physically relevant or robust.

At the decadal timescale, the EMED seems to refer to a pan-Mediterranean SSTa pattern, with very low connections to the North Atlantic (Fig. 4d), unlike at the interannual timescale (Fig. 3d). However, decadal warming (cooling) of the eastern Mediterranean favours (suppressessupresses) deep-convection over most of West Africa, particularly over the Sahel (Fig. 4d), consistent with the pattern at the interannual timescale (Fig. 3d). At the decadal timescale, this is due to a strengthening (weakening) of the Monsoon fluxes, increasing (reducing) convergence with northeasterly fluxes in low-troposphere (Fig. 4d). It is also associated with a decadal weakening (strengthening) of the AEJ, and thus less (more) continental atmospheric moisture exported to the Atlantic (Fig. 4d).

In summary, at the interannual and decadal timescales, while SSTa in the Pacific and the Indian Ocean give insight to large-scale zonal changes in the atmospheric water budget impacting the strength of the WAM, SSTa in the Atlantic and eastern Mediterranean show meridional changes impacting the latitudinal location and strength of the ITCZ and the WAM. However, the link between SSTa in the Indian Ocean (TIO) and the WAM does not appear physically robust at decadal timescales. On the contrary, we note that the SSTa in the eastern Mediterranean (EMED) provide statistically and physically robust information at both interannual and decadal timescales.

4.3. Nonstationary GEV models driven by SST indices

As shown in sections 4.1 and 4.2, ENSO, AtlNiño, TIO and EMED (AMO, AMM, TIO and EMED) significantly contribute to West Africa hydroclimatehydroclimates at interannual (decadal) timescales. Among these SST indices, EMED is the only SST index providing both

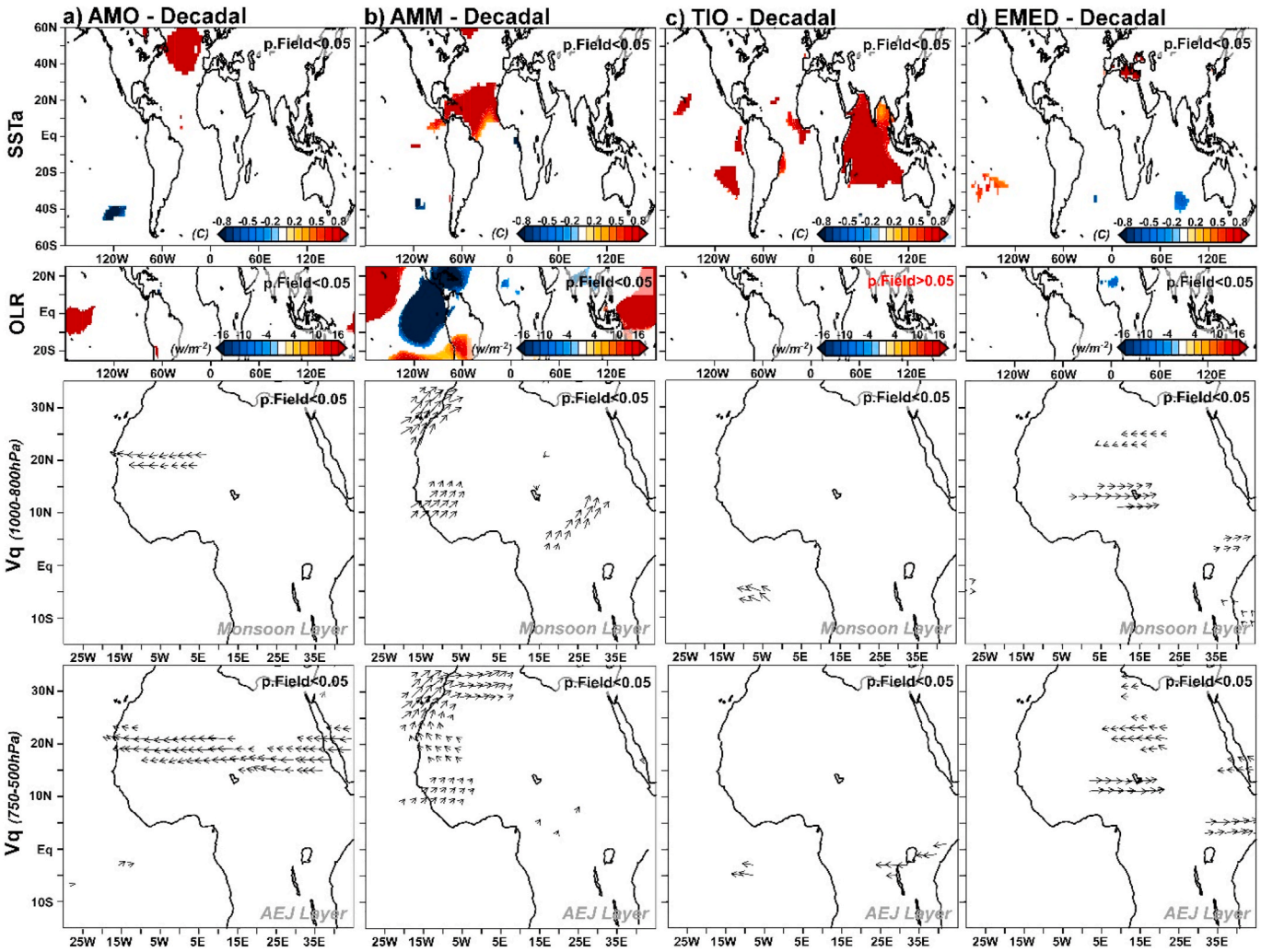

Fig. 4. Same as for Fig. 3 but using the most relevant SST indices (a–d: AMO, AMM, TIO, EMED) and at the decadal timescale (>10 years).

statistically and physically robust information at both interannual and decadal timescales, and showing significant relationships with the GEV scale and location parameters. Therefore, EMED is selected to drive a nonstationary GEV model of streamflow extremes at all stations, except for the Bani Douna model, which is driven by ENSO and the Niger Lokoja model, which is driven by TIO (Figure A2). Here, we only show the results at Koulikoro station in the NRB (Fig. 5). In the stationary extreme analysis, we assume that the parameters of the extreme distribution do not change over time, causing the predicted extreme distribution to remain the same (Fig. 5a). However, the streamflow variability has been demonstrated to be affected by interannual and decadal SST variations, which modulate the moisture circulations (cf. Section 4.1-2). For the nonstationary model, the streamflow extreme distributions shift up and down over time under the effect of EMED, matching well with the streamflow extremes observations (Fig. 5b). Taking the distributions in 1950 and 1980 as examples, respectively, for relatively high-flow and low-flow periods (Fig. 6), the distribution peaks of nonstationary models have good agreement with the observations, whereas the stationary

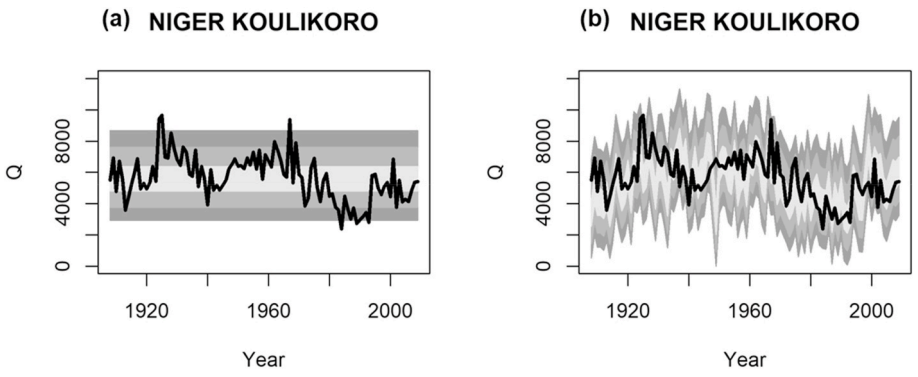

Fig. 5. The stationary (a) and nonstationary extreme analysis driven by EMED (b) in the Niger Koulikoro. The black solid line is the observed streamflow extremes, and the grey-scale bands are the 60th, 80th and 95th percentiles of 1 000 model simulations.

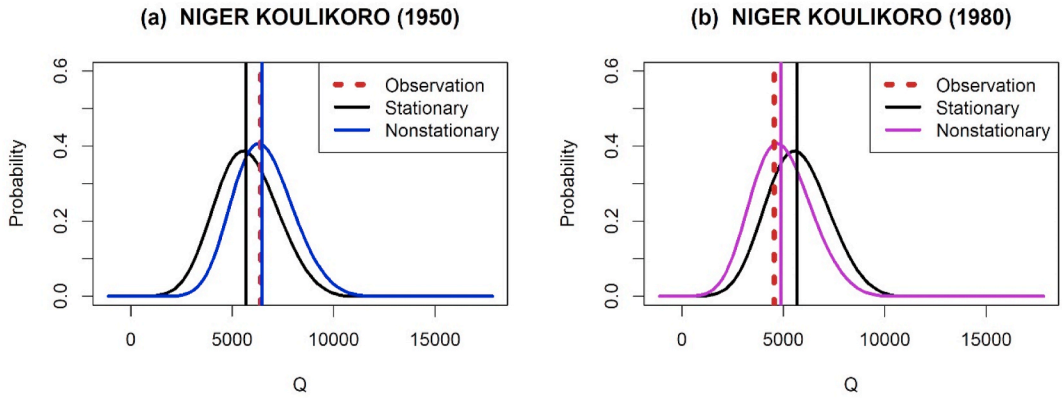

Fig. 6. The extreme distributions from nonstationary and stationary GEV models at 1950 (a) and 1980 (b).

model underestimates (overestimates) the extreme distribution in the 1950s (1980s) due to a cooling (warming) of the EMED region. Figure A3 illustrates further the robustness of the nonstationary extreme analysis using LXOCV (with X equal to 1, 2, 5, 10, 20 and 40, respectively). We note that the larger X is, the more nonstationary results tend to resemble to the stationary results (Figure A3), as less data can be used to estimate nonstationary behaviour. Interestingly, however, the nonstationary extreme modelling is able to predict the recent increase in extreme streamflow at least 10–20 years ahead (Figure A3).

The performance of nonstationary extreme models in predicting streamflow extremes is further validated based on SS_{RMSE} values of nonstationary models driven by EMED, TIO, ENSO and AMO at all stations (Fig. 7). Except for Douna and Lokoja on the NRB, and using TIO and AMO as covariates, respectively (negative value of SS_{RMSE}), the nonstationary models have better or equivalent skills than the stationary models (Fig. 7). The nonstationary model also has better skill when it is driven by EMED compared to other SST indices (Fig. 7). Interestingly, EMED has larger effects over the SRB and upper NRB (Figs. 7a and 1), suggesting the EMED-driven nonstationary extreme models would perform better over the western part, *i.e.* the SRB and the upper NRB.

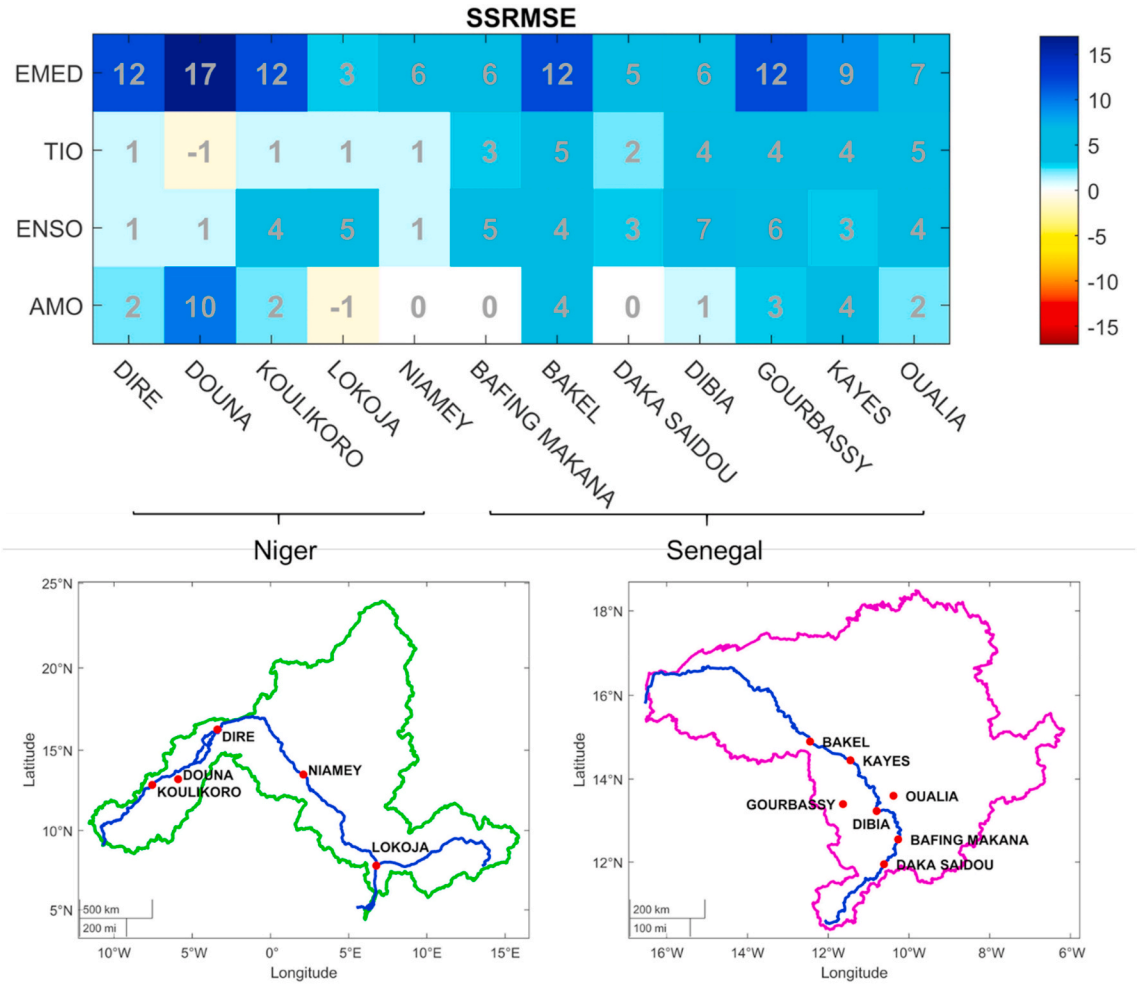

Fig. 7. The SS_{RMSE} of nonstationary extreme models driven by EMED, TIO, ENSO and AMO in NRB and SRB over West Africa.

The other three indices generally contribute more to the predictability of streamflow extremes over the SRB (Fig. 7). As suggested in Section 4.1, this might be due to the catchment size (NRB is larger than the SRB, and thus covers more bio-climatic zones), and as well as the heterogeneity of the NRB (e.g. some impact from the Inner Delta).

5. Conclusion

West Africa has experienced persistent periods with shifts in drought and flood intensity and frequency, which have been proposed to be driven by the combined effects of land-cover change and climate variability (Dai et al., 2004; Dezfuli and Nicholson, 2012). However, while future land-degradation or land-use are highly unpredictable, recent studies suggest that prolonged periods of high-flows or increasing flood frequency could be predicted by monitoring SSTa in the different ocean basins that influence the region's climate (Sidibe et al., 2019). This study thus first examines the contributions of the different ocean basins at both interannual and decadal timescales and their larger-scale mechanisms. The regional streamflow extremes over West Africa are influenced by different modes of SST variability in different Oceans, especially the Atlantic, Pacific, Mediterranean and Indian. While predictability skill is low to moderately good at the interannual timescale, much higher skill is found at decadal timescales, suggesting potential for seamless predictions of prolonged droughts and high-flow conditions over the region. At the interannual timescale, Pacific and Atlantic Niño (i.e., ENSO and AtlNiño), SSTa in the tropical Indian Ocean and eastern Mediterranean (i.e., TIO and EMED) have relatively important impacts on the streamflow extremes over West Africa, whereas, at decadal timescales, SSTa in North and tropical Atlantic, tropical Indian Ocean and eastern Mediterranean (i.e., AMO, AMM, TIO and EMED) have greater contributions. At both the interannual and decadal timescales, while SSTa in the Pacific and the Indian Ocean affect the West Africa hydroclimate by changing the zonal atmospheric moisture impacting the WAM, SSTa in the Atlantic and eastern Mediterranean contribute to meridional changes through modulating the latitudinal shifts and strength of the ITCZ and the WAM. This analysis of the atmospheric dynamic associated with each mode of SST variability is based on the 20CRv3 reanalysis, which was found to represent better decadal Sahel rainfall variability than ERA-20C and CERA-20C (Berntell et al., 2018). Although our results are consistent with previous studies, using various datasets (Grist and Nicholson, 2001; Gouirand et al., 20072; Rowell, 2003; Gaetani et al., 2010; Losada et al., 2010; Mohino et al., 2011; Fontaine et al., 2011; Rodriguez-Fonseca et al., 20110; Dieppois et al., 2013; Sidibe et al., 2019), results could be only slightly different using another century-long reanalysis.

We then integrate the large-scale information, i.e. changes in SSTa in the different ocean basins, in nonstationary extreme modelling. Nonstationary extreme modelling, accounting for temporal changes in flood intensity as a response to different SSTa forcing (e.g. warmer and cooler EMED), is the best performing method, and allows prediction of decadal periods of increasing/decreasing flood intensity, which are crucial for adaptation strategies. Among four SSTa indices, EMED, which has the highest effects on streamflow variability, is the most significant driver based on the nonstationary extreme model results. Other SST indices (ENSO, TIO and AMO) are also significant, but show weaker effects and more spatial variation. However, we note that our seamless extreme modelling strategies perform much better over the SRB than the NRB. This might be due to stronger effects of land-use (-cover) and/or catchment properties (e.g. the Inner Delta) on streamflow in the NRB.

Furthermore, it is expected that the SSTa in different oceans will change as a response to climate change (Deser et al., 2009), and potentially lead to more streamflow extremes by modulating the atmospheric circulation, based on our nonstationary framework for high-flows. Such nonstationary extreme models could also be applied for drought risk assessment. Given the water resource management challenges in West Africa, future work should consider integration of future predictions of multi-year variability in hydrological extremes and extremes-based risk assessment, such as presented here using nonstationary extreme models driven by SST variability. Potential applications include water regulation plans and disaster risk reduction in West Africa, as well as in other regions of the world where there is significant persistence in hydrological behaviour.

CRediT authorship contribution statement

Kwok Pan Chun: Conceptualization, Methodology, Investigation, Software, Resources, Data curation, Formal analysis, Supervision, Writing – review & editing. **Bastien Dieppois:** Data curation, Formal analysis, Writing – review & editing. **Qing He:** Formal analysis, Writing – original draft, Writing – review & editing. **Moussa Sidibe:** Writing – review & editing. **Jonathan Eden:** Writing – review & editing. **Jean-Emmanuel Paturel:** Writing – review & editing. **Gil Mahé:** Writing – review & editing. **Nathalie Rouché:** Writing – review & editing. **Julian Klaus:** Writing – review & editing. **Declan Conway:** Writing – review & editing.

Declaration of competing interest

The authors declare that they have no known competing financial interests or personal relationships that could have appeared to influence the work reported in this paper.

Acknowledgement

This research was conducted using the resources of the High Performance Cluster Computing Centre, Hong Kong Baptist University, which receives funding from Research Grant Council, University Grant Committee of the HKSAR and Hong Kong Baptist University. The extreme approach in the paper was developed from the PROCORE-France/Hong Kong Joint Research Scheme 2020/21 (F-HKBU201/20).

Appendix A. Supplementary data

Supplementary data to this article can be found online at https://doi.org/10.1016/j.wace.2021.100346.

References

Amogu, O., et al., 2010. Increasing river flows in the Sahel? Water 2 (2). https://doi.org/10.3390/w2020170.

Bader, J., Latif, M., 2011. The 1983 drought in the West Sahel: a case study. Clim. Dynam. 36 (3), 463–472. https://doi.org/10.1007/s00382-009-0700-y.

Balas, N., Nicholson, S.E., Klotter, D., 2007. The relationship of rainfall variability in West Central Africa to sea-surface temperature fluctuations. Int. J. Climatol. 27 (10), 1335–1349. https://doi.org/10.1002/joc.1456.

Biasutti, M., Held, I.M., Sobel, A.H., Giannini, A., 2008. SST forcings and Sahel rainfall variability in simulations of the twentieth and twenty-first centuries. J. Clim. 21 (14), 3471–3486. https://doi.org/10.1175/2007JCLI1896.1.

Boyer, J.-F., et al., 2006. SIEREM: an Environmental Information System for Water Resources.

Cai, W., Sullivan, A., Cowan, T., 2009. Rainfall teleconnections with indo-pacific variability in the WCRP CMIP3 models. J. Clim. 22 (19), 5046–5071. https://doi.org/10.1175/2009JCLI2694.1.

Celisse, A., 2014. Optimal cross-validation IN density estimation with the L^2-LOSS. Ann. Stat. 42 (5), 1879–1910.

Cheng, L., AghaKouchak, A., Gilleland, E., Katz, R.W., 2014. Non-stationary extreme value analysis in a changing climate. Climatic Change 127 (2), 353–369. https://doi.org/10.1007/s10584-014-1254-5.

Chiang, J.C.H., Vimont, D.J., 2004. Analogous pacific and atlantic meridional modes of tropical atmosphere–ocean variability. J. Clim. 17 (21), 4143–4158. https://doi.org/10.1175/JCLI4953.1.

Chiew, F.H.S., Piechota, T.C., Dracup, J.A., McMahon, T.A., 1998. El Nino/Southern Oscillation and Australian rainfall, streamflow and drought: links and potential for forecasting. J. Hydrol. 204 (1), 138–149. https://doi.org/10.1016/S0022-1694(97)00121-2.

Coles, S., 2001. Classical extreme value theory and models. In: Coles, S. (Ed.), An Introduction to Statistical Modeling of Extreme Values. Springer London, London, pp. 45–73. https://doi.org/10.1007/978-1-4471-3675-0_3.

Compo, G.P., et al., 2011. The twentieth century reanalysis project. Q. J. R. Meteorol. Soc. 137 (654), 1–28. https://doi.org/10.1002/qj.776.
Dai, A., et al., 2004. The recent Sahel drought is real. Int. J. Climatol. 24 (11), 1323–1331. https://doi.org/10.1002/joc.1083.
Delgado, J.M., Merz, B., Apel, H., 2014. Projecting flood hazard under climate change: an alternative approach to model chains. Nat. Hazards Earth Syst. Sci. 14 (6), 1579–1589. https://doi.org/10.5194/nhess-14-1579-2014.
Delicado, P., Goria, M.N., 2008. A small sample comparison of maximum likelihood, moments and L-moments methods for the asymmetric exponential power distribution. Comput. Stat. Data Anal. 52 (3), 1661–1673. https://doi.org/10.1016/j.csda.2007.05.021.
Descroix, L., et al., 2009. Spatio-temporal variability of hydrological regimes around the boundaries between Sahelian and Sudanian areas of West Africa: a synthesis. J. Hydrol. 375 (1), 90–102. https://doi.org/10.1016/j.jhydrol.2008.12.012.
Descroix, L., et al., 2013. Impact of drought and land–use changes on surface–water quality and quantity: the Sahelian paradox. Current perspectives in contaminant hydrology and water resources sustainability 2, 64.
Deser, C., Alexander, M.A., Xie, S.-P., Phillips, A.S., 2009. Sea surface temperature variability: patterns and mechanisms. Annual Review of Marine Science 2 (1), 115–143. https://doi.org/10.1146/annurev-marine-120408-151453.
Dezfuli, A.K., Nicholson, S.E., 2012. The relationship of rainfall variability in western equatorial Africa to the tropical oceans and atmospheric circulation. Part II: the boreal autumn. J. Clim. 26 (1), 66–84. https://doi.org/10.1175/JCLI-D-11-00686.1.
Dieppois, B., et al., 2013. Quasi-decadal signals of Sahel rainfall and West African monsoon since the mid-twentieth century. J. Geophys. Res.: Atmosphere 118 (22), 12,587–12,599. https://doi.org/10.1002/2013JD019681.
Dieppois, B., et al., 2015a. Low-frequency variability and zonal contrast in Sahel rainfall and Atlantic sea surface temperature teleconnections during the last century. Theor. Appl. Climatol. 121 (1), 139–155. https://doi.org/10.1007/s00704-014-1229-5.
Dieppois, B., Rouault, M., New, M., 2015b. The impact of ENSO on Southern African rainfall in CMIP5 ocean atmosphere coupled climate models. Clim. Dynam. 45 (9), 2425–2442. https://doi.org/10.1007/s00382-015-2480-x.
Ebisuzaki, W., 1997. A method to estimate the statistical significance of a correlation when the data are serially correlated. J. Clim. 10, 2147–2153. https://doi.org/10.1175/1520-0442(1997)010<2147:AMTETS>2.0.CO;2.
Enfield, D.B., Mestas-Nuñez, A.M., Trimble, P.J., 2001. The Atlantic Multidecadal Oscillation and its relation to rainfall and river flows in the continental U.S. Geophys. Res. Lett. 28 (10), 2077–2080. https://doi.org/10.1029/2000GL012745.
Feldman, B., 2005. Relative Importance and Value. Manuscript. SSRN.
Ferro, C.A.T., Segers, J., 2003. Inference for clusters of extreme values. J. Roy. Stat. Soc. B 65 (2), 545–556. https://doi.org/10.1111/1467-9868.00401.
Folland, C.K., Parker, D.E., Colman, A.W., Washington, R., 1999. Large scale modes of ocean surface temperature since the late nineteenth century. In: Navarra, A. (Ed.), Beyond El Niño: Decadal and Interdecadal Climate Variability. Springer Berlin Heidelberg, Berlin, Heidelberg, pp. 73–102. https://doi.org/10.1007/978-3-642-58369-8_4.
Fontaine, B., et al., 2010. Impacts of warm and cold situations in the Mediterranean basins on the West African monsoon: observed connection patterns (1979–2006) and climate simulations. Clim. Dynam. 35 (1), 95–114. https://doi.org/10.1007/s00382-009-0599-3.
Fontaine, B., Monerie, P.-A., Gaetani, M., Roucou, P., 2011. Climate adjustments over the African-Indian monsoon regions accompanying Mediterranean Sea thermal variability. J. Geophys. Res.: Atmosphere 116 (D23). https://doi.org/10.1029/2011JD016273.
Gaetani, M., Fontaine, B., Roucou, P., Baldi, M., 2010. Influence of the Mediterranean Sea on the west african monsoon: intraseasonal variability in numerical simulations. J. Geophys. Res.: Atmosphere 115 (D24). https://doi.org/10.1029/2010JD014436.
Gal, L., Grippa, M., Hiernaux, P., Pons, L., Kergoat, L., 2017. The paradoxical evolution of runoff in the pastoral Sahel: analysis of the hydrological changes over the Agoufou watershed (Mali) using the KINEROS-2 model. Hydrol. Earth Syst. Sci. 21 (9), 4591–4613. https://doi.org/10.5194/hess-21-4591-2017.
García-Serrano, J., Cassou, C., Douville, H., Giannini, A., Doblas-Reyes, F.J., 2017. Revisiting the ENSO teleconnection to the tropical North atlantic. J. Clim. 30 (17), 6945–6957. https://doi.org/10.1175/JCLI-D-16-0641.1.
Gardelle, J., Hiernaux, P., Kergoat, L., Grippa, M., 2010. Less rain, more water in ponds: a remote sensing study of the dynamics of surface water from 1950 to present in pastoral Sahel (Gourma region, Mali). Hydrol. Earth Syst. Sci. 14 (2), 309–324. https://doi.org/10.5194/hess-14-309-2010.
Giannini, A., Saravanan, R., Chang, P., 2005. Dynamics of the boreal summer African monsoon in the NSIPP1 atmospheric model. Clim. Dynam. 25 (5), 517–535. https://doi.org/10.1007/s00382-005-0056-x.
Gouirand, I., Moron, V., Zorita, E., 2007. Teleconnections between ENSO and north atlantic in an ECHO-G simulation of the 1000–1990 period. Geophys. Res. Lett. 34 (6) https://doi.org/10.1029/2006GL028852.
Grist, J.P., Nicholson, S.E., 2001. A study of the dynamic factors influencing the rainfall variability in the west african Sahel. J. Clim. 14 (7), 1337–1359. https://doi.org/10.1175/1520-0442(2001)014<1337:ASOTDF>2.0.CO;2.
Grömping, U., 2007. Estimators of relative importance in linear regression based on variance decomposition. Am. Statistician 61 (2), 139–147. https://doi.org/10.1198/000313007x188252.
Hamatan, M., Mahe, G., Servat, É., Paturel, J.-E., Amani, A., 2004. Synthèse et évaluation des prévisions saisonnières en Afrique de l'Ouest. Sci. Chang. Planétaires Sécher. 15 (3), 279–286.
Hawkes, P.J., Gonzalez-Marco, D., Sánchez-Arcilla, A., Prinos, P., 2008. Best practice for the estimation of extremes: a review. J. Hydraul. Res. 46 (Suppl. 2), 324–332. https://doi.org/10.1080/00221686.2008.9521965.
Hosking, J.R.M., 1990. L-moments: analysis and estimation of distributions using linear combinations of order statistics. J. Roy. Stat. Soc. B 52 (1), 105–124. https://doi.org/10.1111/j.2517-6161.1990.tb01775.x.
Huang, B., et al., 2017. Extended reconstructed sea surface temperature, version 5 (ERSSTv5): upgrades, validations, and intercomparisons. J. Clim. 30 (20), 8179–8205.
Jolliffe, I.T., Stephenson, D.B., 2012. Forecast Verification: a Practitioner's Guide in Atmospheric Science. John Wiley & Sons.
Katz, R.W., Parlange, M.B., Naveau, P., 2002. Statistics of extremes in hydrology. Adv. Water Resour. 25 (8), 1287–1304. https://doi.org/10.1016/S0309-1708(02)00056-8.
Kotz, S., Nadarajah, S., 2000. Extreme Value Distributions. PUBLISHED BY IMPERIAL COLLEGE PRESS AND DISTRIBUTED BY WORLD SCIENTIFIC PUBLISHING CO., p. 196. https://doi.org/10.1142/p191
Laloyaux, P., et al., 2018. CERA-20C: a coupled reanalysis of the twentieth century. J. Adv. Model. Earth Syst. 10 (5), 1172–1195. https://doi.org/10.1029/2018MS001273.
Lebel, T., Ali, A., 2009. Recent trends in the central and western Sahel rainfall regime (1990–2007). J. Hydrol. 375 (1), 52–64. https://doi.org/10.1016/j.jhydrol.2008.11.030.
Lehner, B., et al., 2011. High-resolution mapping of the world's reservoirs and dams for sustainable river-flow management. Front. Ecol. Environ. 9 (9), 494–502. https://doi.org/10.1890/100125.
Lima, C.H.R., Lall, U., 2010. Spatial scaling in a changing climate: a hierarchical bayesian model for non-stationary multi-site annual maximum and monthly streamflow. J. Hydrol. 383 (3), 307–318. https://doi.org/10.1016/j.jhydrol.2009.12.045.
Lindeman, R.H., Merenda, P.F., Gold, R.Z., 1980. Introduction to Bivariate and Multivariate Analysis. Glenview.
Losada, T., et al., 2010. A multi-model approach to the Atlantic Equatorial mode: impact on the West African monsoon. Clim. Dynam. 35 (1), 29–43. https://doi.org/10.1007/s00382-009-0625-5.
Lu, J., Delworth, T.L., 2005. Oceanic forcing of the late 20th century Sahel drought. Geophys. Res. Lett. 32 (22) https://doi.org/10.1029/2005GL023316.
Lü, M., et al., 2018. Changes in extreme precipitation in the Yangtze River basin and its association with global mean temperature and ENSO. Int. J. Climatol. 38 (4), 1989–2005. https://doi.org/10.1002/joc.5311.
Mahé, G., Citeau, J., 1993. Interactions between the ocean, atmosphere and continent in Africa, related to the Atlantic monsoon flow. General pattern and the 1984 case study. Veille Clim. Satell 44, 34–54.
Mahe, G., et al., 2013. The rivers of Africa: witness of climate change and human impact on the environment. Hydrol. Process. 27 (15), 2105–2114. https://doi.org/10.1002/hyp.9813.
Mahé, G., Paturel, J.-E., 2009. 1896–2006 Sahelian annual rainfall variability and runoff increase of Sahelian Rivers. Compt. Rendus Geosci. 341 (7), 538–546. https://doi.org/10.1016/j.crte.2009.05.002.
Mantua, N.J., Hare, S.R., Zhang, Y., Wallace, J.M., Francis, R.C., 1997. A pacific interdecadal climate oscillation with impacts on salmon production*. Bull. Am. Meteorol. Soc. 78 (6), 1069–1080. https://doi.org/10.1175/1520-0477(1997)078<1069:APICOW>2.0.CO;2.
Maraun, D., Rust, H.W., Osborn, T.J., 2010. Synoptic airflow and UK daily precipitation extremes. Extremes 13 (2), 133–153. https://doi.org/10.1007/s10687-010-0102-x.
Martins, E.S., Stedinger, J.R., 2000. Generalized maximum-likelihood generalized extreme-value quantile estimators for hydrologic data. Water Resour. Res. 36 (3), 737–744. https://doi.org/10.1029/1999WR900330.
Masih, I., Maskey, S., Mussá, F.E.F., Trambauer, P., 2014. A review of droughts on the African continent: a geospatial and long-term perspective. Hydrol. Earth Syst. Sci. 18 (9), 3635–3649. https://doi.org/10.5194/hess-18-3635-2014.
Mohino, E., Janicot, S., Bader, J., 2011. Sahel rainfall and decadal to multi-decadal sea surface temperature variability. Clim. Dynam. 37 (3), 419–440. https://doi.org/10.1007/s00382-010-0867-2.
Nicholson, S., 2005. On the question of the "recovery" of the rains in the West African Sahel. J. Arid Environ. 63 (3), 615–641. https://doi.org/10.1016/j.jaridenv.2005.03.004.
Nicholson, S.E., Some, B., Kone, B., 2000. An analysis of recent rainfall conditions in West Africa, including the rainy seasons of the 1997 El Niño and the 1998 La niña years. J. Clim. 13 (14), 2628–2640. https://doi.org/10.1175/1520-0442(2000)013<2628:AAORRC>2.0.CO;2.
Olivry, J.-C., 2002. Synthèse des connaissances hydrologiques et potentiel en ressources en eau du fleuve Niger. World Bank, Niger Basin Authority, p. 160 provisional report.
Oyerinde, G.T., et al., 2015. Hydro-climatic changes in the Niger basin and consistency of local perceptions. Reg. Environ. Change 15 (8), 1627–1637. https://doi.org/10.1007/s10113-014-0716-7.
Pisarenko, V., Rodkin, M., 2010. Models for the generation of distributions of different types. In: Pisarenko, V., Rodkin, M. (Eds.), Heavy-Tailed Distributions in Disaster Analysis. Springer Netherlands, Dordrecht, pp. 23–37. https://doi.org/10.1007/978-90-481-9171-0_2.
Poccard, I., Janicot, S., Camberlin, P., 2000. Comparison of rainfall structures between NCEP/NCAR reanalyses and observed data over tropical Africa. Clim. Dynam. 16 (12), 897–915. https://doi.org/10.1007/s003820000087.
Pohl, B., Dieppois, B., Crétat, J., Lawler, D., Rouault, M., 2018. From synoptic to interdecadal variability in southern african rainfall: toward a unified view across time scales. J. Clim. 31 (15), 5845–5872. https://doi.org/10.1175/JCLI-D-17-0405.1.
Poli, P., et al., 2016. ERA-20C: an atmospheric reanalysis of the twentieth century. J. Clim. 29 (11), 4083–4097. https://doi.org/10.1175/JCLI-D-15-0556.1.

Power, S., Casey, T., Folland, C., Colman, A., Mehta, V., 1999. Inter-decadal modulation of the impact of ENSO on Australia. Clim. Dynam. 15 (5), 319–324. https://doi.org/10.1007/s003820050284.
Reynolds, R.W., Rayner, N.A., Smith, T.M., Stokes, D.C., Wang, W., 2002. An improved in situ and satellite SST analysis for climate. J. Clim. 15 (13), 1609–1625. https://doi.org/10.1175/1520-0442(2002)015<1609:AIISAS>2.0.CO;2.
Rodríguez-Fonseca, B., et al., 2011. Interannual and decadal SST-forced responses of the West African monsoon. Atmos. Sci. Lett. 12 (1), 67–74. https://doi.org/10.1002/asl.308.
Rodríguez-Fonseca, B., et al., 2015. Variability and predictability of West african droughts: a review on the role of sea surface temperature anomalies. J. Clim. 28 (10), 4034–4060. https://doi.org/10.1175/JCLI-D-14-00130.1.
Roudier, P., Ducharne, A., Feyen, L., 2014. Climate change impacts on runoff in West Africa: a review. Hydrol. Earth Syst. Sci. 18, 2789–2801. https://doi.org/10.5194/hess-18-2789-2014.
Rowell, D.P., 2001. Teleconnections between the tropical pacific and the Sahel. Q. J. R. Meteorol. Soc. 127 (575), 1683–1706. https://doi.org/10.1002/qj.49712757512.
Rowell, D.P., 2003. The impact of mediterranean SSTs on the sahelian rainfall season. J. Clim. 16 (5), 849–862. https://doi.org/10.1175/1520-0442(2003)016<0849:tiomso>2.0.co;2.
Rust, H.W., Maraun, D., Osborn, T.J., 2009. Modelling seasonality in extreme precipitation. Eur. Phys. J. Spec. Top. 174 (1), 99–111. https://doi.org/10.1140/epjst/e2009-01093-7.
Saji, N.H., Xie, S.P., Yamagata, T., 2006. Tropical Indian ocean variability in the IPCC twentieth-century climate simulations. J. Clim. 19 (17), 4397–4417. https://doi.org/10.1175/JCLI3847.1.
Schlather, M., 2002. Models for stationary max-stable random fields. Extremes 5 (1), 33–44. https://doi.org/10.1023/A:1020977924878.
Schlef, K.E., François, B., Robertson, A.W., Brown, C., 2018. A general methodology for climate-informed approaches to long-term flood projection—illustrated with the Ohio river basin. Water Resour. Res. 54 (11), 9321–9341. https://doi.org/10.1029/2018WR023209.
Séguis, L., et al., 2011. Contrasted land-surface processes along the West African rainfall gradient. Atmos. Sci. Lett. 12 (1), 31–37. https://doi.org/10.1002/asl.327.
Séguis, L., et al., 2004. Simulated impacts of climate change and land-clearing on runoff from a small Sahelian catchment. Hydrol. Process. 18 (17), 3401–3413. https://doi.org/10.1002/hyp.1503.
Séguis, L., Cappelaere, B., Peugeot, C., Vieux, B., 2002. Impact on Sahelian runoff of stochastic and elevation-induced spatial distributions of soil parameters. Hydrol. Process. 16 (2), 313–332. https://doi.org/10.1002/hyp.337.
Sidibe, M., et al., 2019. Interannual to Multi-decadal streamflow variability in West and Central Africa: interactions with catchment properties and large-scale climate variability. Global Planet. Change 177, 141–156. https://doi.org/10.1016/j.gloplacha.2019.04.003.
Sidibe, M., et al., 2018. Trend and variability in a new, reconstructed streamflow dataset for West and Central Africa, and climatic interactions, 1950–2005. J. Hydrol. 561, 478–493. https://doi.org/10.1016/j.jhydrol.2018.04.024.
Sighomnou, D., et al., 2013. La crue de 2012 à Niamey : un paroxysme du paradoxe du Sahel ? Sci. Chang. Planétaires Sécher. 24 (1), 3–13. https://doi.org/10.1684/sec.2013.0370.
Slivinski, L.C., et al., 2019. Towards a more reliable historical reanalysis: improvements for version 3 of the Twentieth Century Reanalysis system. Q. J. R. Meteorol. Soc. 145 (724), 2876–2908. https://doi.org/10.1002/qj.3598.
Šraj, M., Viglione, A., Parajka, J., Blöschl, G., 2016. The influence of non-stationarity in extreme hydrological events on flood frequency estimation. J. Hydrol. Hydromechanics 64 (4), 426–437. https://doi.org/10.1515/johh-2016-0032.
Tao, Y., et al., 2014. An evaluation of post-processed TIGGE multimodel ensemble precipitation forecast in the Huai river basin. J. Hydrol. 519, 2890–2905. https://doi.org/10.1016/j.jhydrol.2014.04.040.
Tarhule, A., 2005. Damaging rainfall and flooding: the other Sahel hazards. Climatic Change 72 (3), 355–377. https://doi.org/10.1007/s10584-005-6792-4.
Taylor, C.M., et al., 2017. Frequency of extreme Sahelian storms tripled since 1982 in satellite observations. Nature 544 (7651), 475–478. https://doi.org/10.1038/nature22069.
Tošić, I., Unkašević, M., Putniković, S., 2017. Extreme daily precipitation: the case of Serbia in 2014. Theor. Appl. Climatol. 128 (3), 785–794. https://doi.org/10.1007/s00704-016-1749-2.
Tramblay, Y., Amoussou, E., Dorigo, W., Mahé, G., 2014. Flood risk under future climate in data sparse regions: linking extreme value models and flood generating processes. J. Hydrol. 519, 549–558. https://doi.org/10.1016/j.jhydrol.2014.07.052.
Trenberth, K.E., Shea, D.J., 2006. Atlantic hurricanes and natural variability in 2005. Geophys. Res. Lett. 33 (12) https://doi.org/10.1029/2006GL026894.
Tyralis, H., Papacharalampous, G., Tantanee, S., 2019. How to explain and predict the shape parameter of the generalized extreme value distribution of streamflow extremes using a big dataset. J. Hydrol. 574, 628–645. https://doi.org/10.1016/j.jhydrol.2019.04.070.
Vicente-Serrano, S.M., et al., 2012. Challenges for drought mitigation in Africa: the potential use of geospatial data and drought information systems. Appl. Geogr. 34, 471–486. https://doi.org/10.1016/j.apgeog.2012.02.001.
Weller, E., Cai, W., 2013. Asymmetry in the IOD and ENSO teleconnection in a CMIP5 model ensemble and its relevance to regional rainfall. J. Clim. 26 (14), 5139–5149. https://doi.org/10.1175/JCLI-D-12-00789.1.
Wilby, R.L., Quinn, N.W., 2013. Reconstructing multi-decadal variations in fluvial flood risk using atmospheric circulation patterns. J. Hydrol. 487, 109–121. https://doi.org/10.1016/j.jhydrol.2013.02.038.
Wilcox, C., et al., 2018. Trends in hydrological extremes in the Senegal and Niger Rivers. J. Hydrol. 566, 531–545. https://doi.org/10.1016/j.jhydrol.2018.07.063.
Wilks, D.S., 2006. On "field significance" and the false discovery rate. Journal of Applied Meteorology and Climatology 45 (9), 1181–1189. https://doi.org/10.1175/JAM2404.1.
Wilks, D.S., 2016. "The stippling shows statistically significant grid points": how research results are routinely overstated and overinterpreted, and what to do about it. Bull. Am. Meteorol. Soc. 97 (12), 2263–2273. https://doi.org/10.1175/BAMS-D-15-00267.1.
Wohland, J., Omrani, N.-E., Witthaut, D., Keenlyside, N.S., 2019. Inconsistent wind speed trends in current twentieth century reanalyses. J. Geophys. Res.: Atmosphere 124 (4), 1931–1940. https://doi.org/10.1029/2018JD030083.
Wu, Z., Huang, N.E., Long, S.R., Peng, C.-K., 2007. On the trend, detrending, and variability of nonlinear and nonstationary time series. Proc. Natl. Acad. Sci. Unit. States Am. 104 (38), 14889. https://doi.org/10.1073/pnas.0701020104.
Zhang, X., Wang, J., Zwiers, F.W., Groisman, P.Y., 2010. The influence of large-scale climate variability on winter maximum daily precipitation over North America. J. Clim. 23 (11), 2902–2915. https://doi.org/10.1175/2010JCLI3249.1.
Zhang, Z., et al., 2011. Evaluating the non-stationary relationship between precipitation and streamflow in nine major basins of China during the past 50 years. J. Hydrol. 409 (1), 81–93. https://doi.org/10.1016/j.jhydrol.2011.07.041.